

Imaging Motional Stark Effect measurements at ASDEX Upgrade

O. P. Ford,¹ A. Burckhart,¹ R. McDermott,¹ R. Wolf,¹ and the ASDEX Upgrade Team¹
Max-Planck Institut für Plasmaphysik, Greifswald/Garching, Germany

This paper presents an overview of results from the Imaging Motional Stark Effect (IMSE) diagnostic obtained during its first measurement campaign at ASDEX Upgrade since installation as a permanent diagnostic. A brief overview of the general IMSE technique is given, followed by some specifics of the new permanent IMSE system. Measurements of a standard H-mode discharge are compared to equilibrium reconstructions showing good agreement where expected. The calibration and compensation of Faraday rotation and the development of special discharges for the calibration of pitch angle are reported. Finally, safety factor profiles changes during sawteeth crashes are shown, which can be resolved to a few percent due to the high sensitivity at good time resolution of the new IMSE system.

I. Introduction

The determination of the current density profile of modern Tokamak plasmas remains a significant challenge and the Motional Stark Effect (MSE) polarimetry technique¹ remains one of the most productive diagnostics. MSE diagnostics collect H/D α emission from a beam of neutral hydrogen or deuterium particles injected at high energy. H α line emission is Stark-split by the local magnetic field, which is seen as an electric field in the rest frame of the particle. The polarisation states of the resulting multiplet components are aligned parallel or perpendicular to this field, so carry information about the magnetic field pitch angle. A typical MSE system uses a Photo Elastic Modulator (PEM) and polariser to temporally modulate the light intensity according to the polarisation state and digitises the signal using a photomultiplier tube or photodiode. A narrow inference filter is required to select either the σ or π component of the MSE multiplet due to their orthogonal polarisations. The filter must be carefully tilt and temperature tuned as the Doppler shifted wavelength varies with spatial channel. The requirement of separate filtering and detection hardware for each channel strongly limits the quantity of information that can be collected.

II. Imaging Motional Stark Effect at ASDEX Upgrade

The Imaging MSE (IMSE) system² uses a CCD/CMOS camera to capture a 2D image of the neutral beam and a set of birefringent plates and polariser to modulate the image spatially with interference patterns that encode the polarisation state. A typical raw image can be seen in figure 1a. The interference patterns have a strongly wavelength dependent phase, chosen such that all of the Stark multiplet transitions add constructively, despite their orthogonal polarisations. This removes the need for narrow optical filters and allows the use of all of the available light. Coupled with the high speed, sensitivity and useful area of modern imaging cameras, the 2D image provides superior signal/noise and at least an order of magnitude more data than a typical MSE diagnostic.

To investigate the capabilities of IMSE, a compact prototype system was developed for ASDEX Upgrade³, thoroughly tested and installed in place of the classical MSE

polarimeter for several weeks. After promising results⁴, a permanent IMSE system was installed. For the first phase, the existing prototype 'back-end' was installed on a new dedicated set of optics⁵. The calibration, first results and performance of the new system are documented here. The details of the back-end can be found elsewhere³.

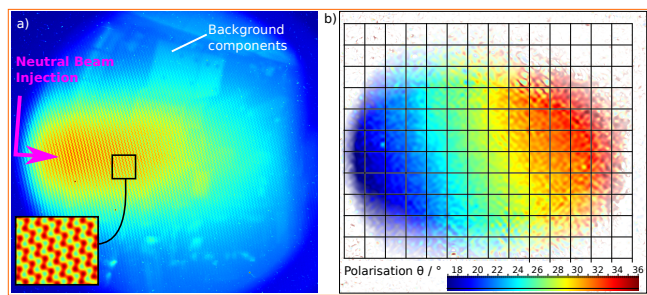


FIG. 1. a) Raw IMSE image and b) demodulated polarisation angle image for a single time point of a reference H-mode discharge. The polarisation angle image is intensity blended according to the uncertainty estimate calculated from CCD shot-noise.

III. Optics

The set-up of the permanent IMSE is shown in figure 2. A series of six lenses and three dielectric mirrors image 60cm of three neutral beam sources onto a 20mm virtual image in front of the IMSE back-end with a full image étendue of over $30\text{mm}^2\text{sr}$. The prototype back-end accepts only $11\text{mm}^2\text{sr}$ but will be replaced in the next campaign with a design capable of accepting at least $20\text{mm}^2\text{sr}$. The view position was chosen to give the best compromise of Doppler shift, pitch angle sensitivity and mechanical feasibility. The port is shared with several other diagnostics and the optical components fit around the ICRH antenna, lithium beam and IR thermography tubes, while avoiding the lines of sight of the electron cyclotron emission (ECE) and neutron monitor diagnostics. The steep angle of the light relative to the port flange requires a further dual-mirror box to avoid a large poloidal field coil support structure. Despite the complexity, lab tests confirmed that the optical chain preserves linearity of the polarisation state to within $\pm 0.1^\circ$ over the required

wavelength range $650\text{nm} < \lambda < 654\text{nm}$.

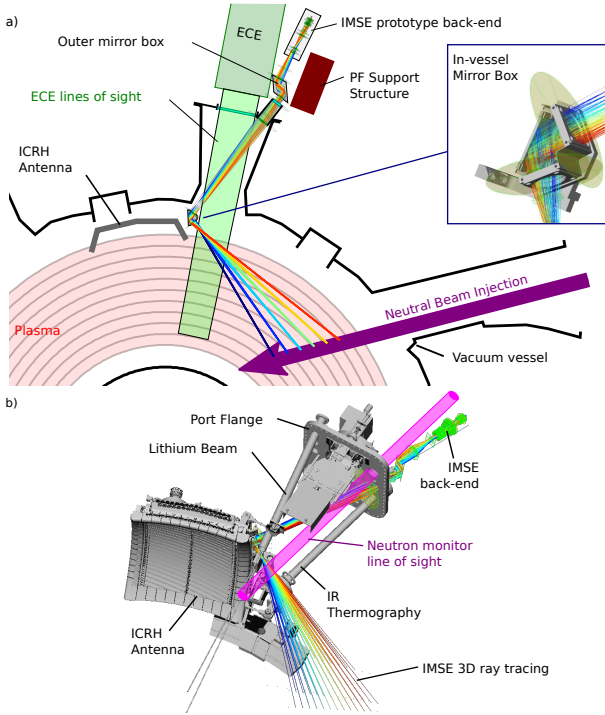


FIG. 2. a) Over-head schematic and b) CAD view of the ASDEX upgrade permanent IMSE diagnostic

IV. Initial Results, comparison to equilibrium predictions.

Figure 1 shows a raw CCD image and demodulated polarisation angle image from a standard H-mode discharge, which are repeated weekly at ASDEX Upgrade. Since spatial resolution is in any case limited by integration across flux surfaces through the depth of the neutral beam, a grid of 15×12 blocks is averaged and used for further analysis without significant loss of information. Figure 3 shows time traces of 6 blocks during a standard H-Mode shot. In total, the IMSE delivers at least 100 of these independent data points at the noise level shown, an order of magnitude improvement over the traditional MSE systems.

Unfortunately, as the outer mirror box and back-end mount were not available before the closing of the vacuum vessel, no internal calibration could be performed. Instead, the time traces are adjusted by an offset to highlight the very good agreement of the time evolution with that predicted from an equilibrium reconstruction (magnetics-only). Significant deviation is seen only at the end of the discharge when sawteeth cycles appear, which the equilibrium code is unable to predict.

Figure 4 shows a profile taken from the image (blue) versus major radius compared with the equilibrium prediction. In this case, adjusting the prediction by a linear function of radius is sufficient and the remaining curvature matches that calculated from the equilibrium. The profile of the difference between two time points of the

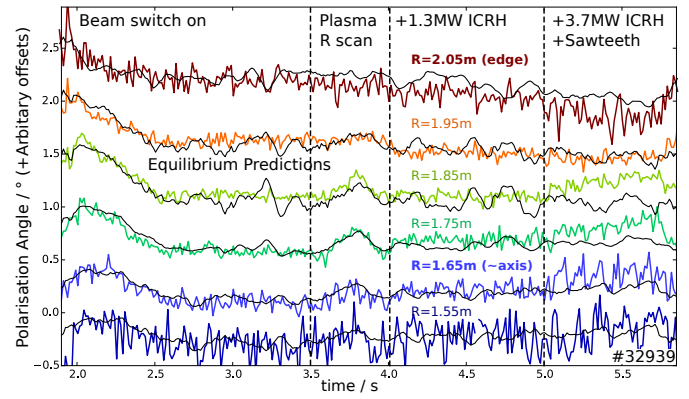


FIG. 3. Time evolution of measured polarisation angle at 6 radial locations during an ASDEX-Upgrade reference H-Mode discharge. Also shown are the predictions from the equilibrium code CLISTE (magnetics only) including Faraday rotation and radial electric field corrections. Offsets of all traces are set arbitrarily to match predictions and to simplify the graph.

discharge, shown in black, requires no offsets and shows good agreement with the prediction.

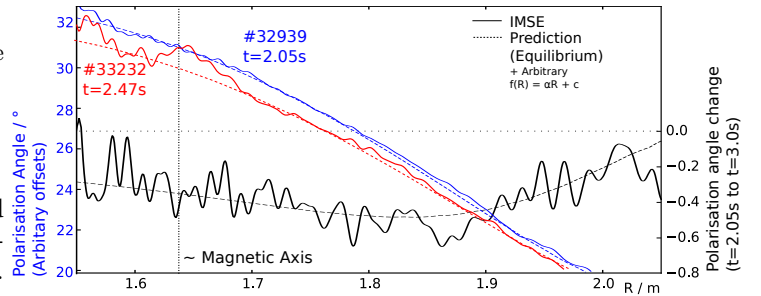


FIG. 4. Blue: Radial profile of the measured IMSE data at 2.05s in a good reference H-Mode discharge, with equilibrium prediction. Prediction is modified by an arbitrary linear offset to match measurements. Black: Profile of predicted and measured difference between time points $t=3.00\text{s}$ and $t=2.05\text{s}$ showing the evolution after switch-on of the neutral beam. Red: Later reference H-mode discharge showing disturbances to core data.

Unfortunately, for much of the data taken in the first campaign, a disturbance to the core data ($R < 1.7\text{m}$) is present. The cause is not yet confirmed, but is most likely the result of a reflection in the optical relay system, since only optical alignment adjustments modified the disturbance. A critical possibility would have been a complex interaction of the spectral optimisation (as described in³) but this was excluded by showing that the spectral distribution, which was modified by changes of beam energy and band-pass filter incidence angle, does not alter the disturbance. An attempt to isolate the source will be made once the vacuum vessel is opened. In the meantime, since the cause is likely to be interference from light belonging to a different radius, the data in ($R < 1.7\text{m}$)

cannot be trusted.

V. Faraday Rotation

Although the optical system was mostly made from a special low-Verdet constant glass, some fused silica components were required⁵. Furthermore, the prototype back-end uses a large commercial objective lens which contains glasses of unknown Verdet constant. To assess the resulting Faraday effect, a small polarised calibration source was installed at the vessel wall in the IMSE field of view and used to measure the Faraday rotation during a magnetic field coil test shot (no plasma). The ray tracing code developed for the design of the IMSE system is used to calculate the Faraday rotation, allowing one free parameter for the Verdet constant of the commercial lens. The resulting fit and the measurement are shown in figure 5. An independent measurement using a polariser and calibration sphere in front of the back-end during the coil test confirms that there is no field of view dependence. During plasma measurements, the Faraday rotation can now be reliably corrected to an accuracy of $\delta\theta < \pm 0.02^\circ$.

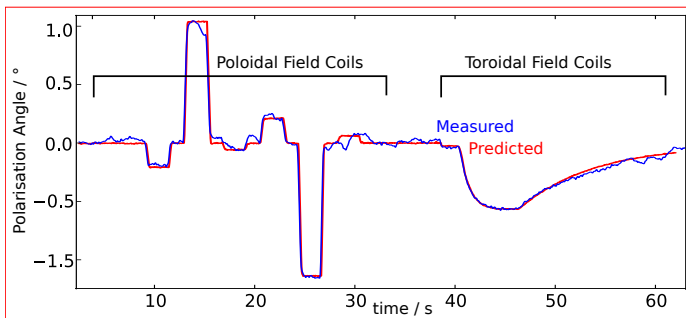


FIG. 5. Measured (blue) and modelled (red) polarisation change due to Faraday rotation in optical components resulting from changes in the poloidal toroidal field coils.

VI. Reverse Bt calibration

The measured polarisation angle θ is approximately linearly related to the pitch angle by the pitch angle sensitivity α , which is determined from the beam and view geometry. For the permanent IMSE system⁵ this lies in the range $0.4 < \alpha < 0.6$.

$$\theta - \theta_c \approx \alpha B_z / B_\phi \quad (1)$$

In order to calibration the offset θ_c , a pair of otherwise similar discharges were developed with normal and reversed toroidal field B_ϕ but the same plasma current direction. The average of the two shots should approximately give θ_c , the polarisation of zero pitch and the position at which the polarisation is unchanged by reversal of B_ϕ should be that of the magnetic axis. To check this, the magnetic axis position is scanned slowly over the range $1.70 < R_0 < 1.74m$. Figure 6 shows the polarisation profiles recorded during the position scan for both positive and negative B_ϕ .

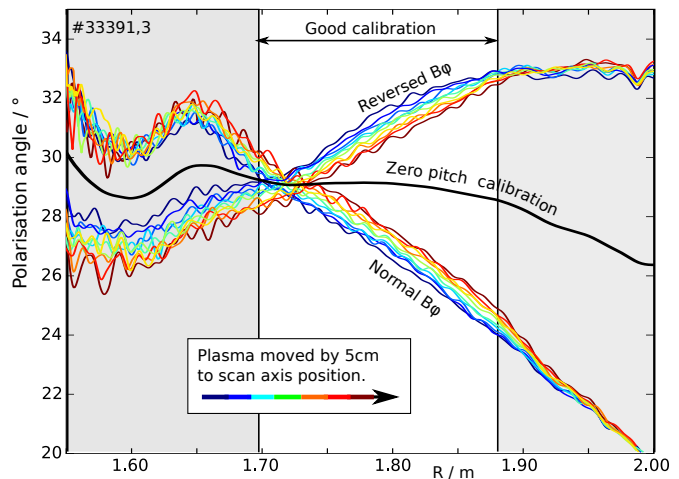


FIG. 6. Measured profiles of polarisation angle during a position scan of similar plasmas with normal and reversed toroidal field, faraday rotation corrected. The crossing points of +ve and -ve B_ϕ should coincide with the magnetic axis.

Again, the effect of the disturbance can clearly be seen for $R < 1.7m$, particularly for the normal B_ϕ direction. Outside $R \approx 1.87m$, the clear linear movement of the plasma is no longer seen and the calibration method should not be considered valid. At this distance from the axis, the linear dependence on the pitch angle is no longer valid. Additionally, the linearity of the diagnostic can not be trusted over the 10° difference due to the as-yet uncompensated intrinsic contrast effect (see³). Within the core region, the radial position of the crossing point can be seen to move outward during the position scan. Figure 7 shows the surprisingly good agreement between the crossing point as determined from a linear fit of each profile within $1.69 < R_0 < 1.78m$, with that predicted by the equilibrium code.

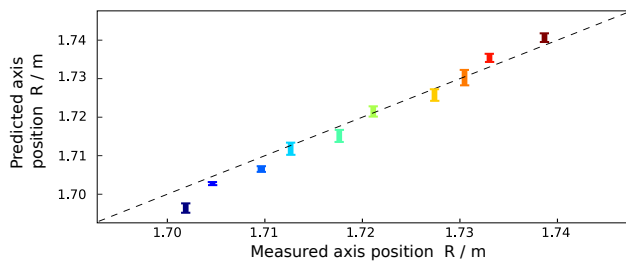


FIG. 7. Magnetic axis position according to equilibrium reconstruction vs measured crossing point of polarisation profiles for normal and reversed toroidal field. Prediction is shown as the range between that for the normal and reversed B_ϕ discharges.

As the field line pitch angle of the reversed B_ϕ is incompatible with the lower divertor, reversed B_ϕ discharges at ASDEX Upgrade must use an upper single null plasma. In this configuration, the axis position scan can not cover the usual axis position of $R \approx 1.65m$, where the calibra-

tion is most desirable, but the disturbance currently prohibits calibration in this region in any case. The upper single null configuration also uses the rarely used open upper divertor, giving difficulty in controlling the plasma density and impurity content and hence in producing identical shots. Finally, the L-H transition threshold in the upper-single null configuration is higher for normal B_ϕ than reversed due to the unfavourable grad-B drift direction. To achieve similar conditions in both discharges, care must be taken that both remain in H-mode and that the initial transition is made rapidly.

VII. Sawtooth Dynamics

The large quantity of low noise measurements allows the inference of very small changes in the current profile, such as during the sawtooth crash⁶⁻⁸. With a reliable calibration procedure, it will be possible to include the IMSE data as constraints in an equilibrium reconstruction. However, it is difficult to see in such reconstructions what is inferred from the data, and what comes from the assumptions of the equilibrium code. Instead, an approximation of the toroidal current density j_ϕ can be calculated directly⁹ from the radial derivative of B_z (equation 2). B_z is determined from the polarisation angle θ , the calibration θ_c (figure 6, black) and the vacuum toroidal field B_ϕ using equation 1.

$$\mu_0 J_\phi = - \left(1 + \frac{1}{\kappa^2} \right) \frac{\partial B_z}{\partial R} \quad (2)$$

The elongation profile $\kappa(R)$ can be taken from the standard equilibrium reconstruction as κ is a weak function of R and does not change significantly in time.

The quantity of most interest in the sawtooth crash is the central safety factor q_0 ⁶⁻⁸. From the large aspect ratio approximation $q_0 \sim 2B_\phi / \mu_0 j_\phi R_0$, it can be seen that small changes $\Delta q_0 \ll 1$ near $q_0 \sim 1.0$ as are expected for sawteeth, are approximately linearly related to the radial derivative of the polarisation angle. To illustrate the importance of the IMSE's high sensitivity, figure 8 compares the difference between neighbouring core channels (ΔR 4cm) of the PEM based MSE polarimeter to the difference between block averages of equivalent areas of the IMSE image. While changes can be clearly seen in the IMSE signal, the signal/noise of the PEM based MSE is far too low to resolve them.

Motivated by this, IMSE pitch angle profiles from a shot with large consistent sawteeth were averaged into 10 profiles according to their phase in the sawtooth cycle, as determined from the soft X-ray diagnostic. Pitch angles were calculated after correcting for Faraday rotation and radial electric field and the current density profiles derived using equation 2 are shown in figure 9. The redistribution of current at the crash from the core region to outside an inversion radius of $R \sim 1.83m$ is very clear. This is followed by a gradual rebuilding of the central current density. Unfortunately, due the disturbance described in section IV, the absolute value and profile shape of the important core region cannot be used.

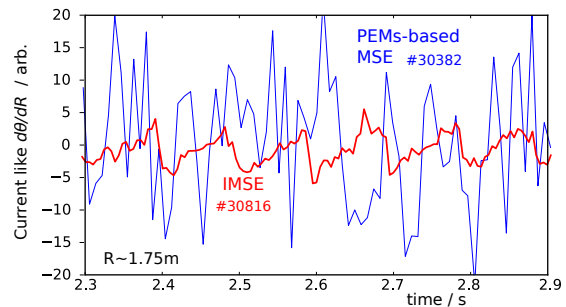


FIG. 8. Current-like quantity calculated from the difference between polarisation angle of two radial channels of the PEM based MSE polarimeter (blue) and of equivalent areas of the IMSE image (red) near the plasma core during sawteeth.

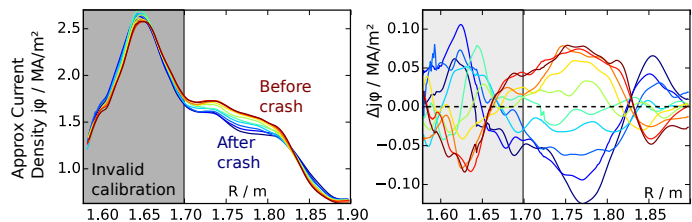


FIG. 9. a) Evolution of the toroidal current density profile j_ϕ during sawteeth as derived from IMSE polarisation angle images using equation 9. Each profile is the average of 1/10th of the sawtooth cycle over 40 sawteeth crashes. Spatial smoothing with length scale 4cm is also applied to reduce noise. b) Profiles relative to the average, showing the maximum change.

If the current density profile is not strongly peaked at the magnetic axis, the large aspect approximation for q_0 remains approximately valid in the vicinity, at least well enough to show the magnitude of changes in q . Figure 10 shows Δq at the location of strongest change $R = 1.77m$ to demonstrate that at a spatial resolution of 5cm and time resolution of 5.7ms, the IMSE has sufficiently low noise to resolve dynamics of the safety factor profile Δq to within a few percent.

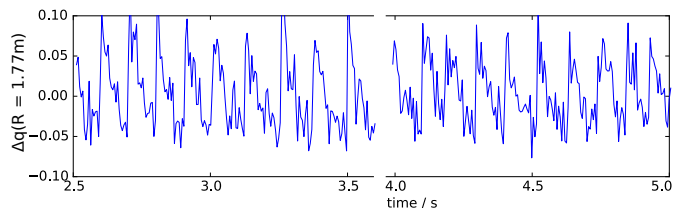


FIG. 10. Approximate changes in q at $R = 1.76m$. The values are only indicative of the magnitude of changes due to the strong assumptions made in the calculation.

VIII. Summary

The Imaging Motional Start Effect diagnostic has been installed at ASDEX Upgrade using a new optical relay system. Initial results show good agreement with plasma

pitch angle changes predicted by equilibrium reconstruction. A calibration method was successfully developed to remove Faraday rotation changes caused by high Verdet constant glass. A new calibration method to determine the polarisation angle of zero zero pitch is under development and shows good agreement with predictions of the magnetic axis position. A disturbance, probably caused by stray reflections currently prohibits a complete calibration of the system. Using the new high precision measurements provided by the IMSE, the redistribution of current during sawteeth crashes can be clearly seen in profiles derived directly from the raw data. Dynamics in the safety factor profile can now be observed within a few percent on less than 10ms timescales. This represents a significant improvement in the diagnostic capability of core Tokamak current density. In future work, the forward/reverse B_ϕ calibration method will be further developed and compared with an absolute in-vessel calibration. A new back-end will also be installed to improve the diagnostic stability and sensitivity even further.

IX. Acknowledgement

The author would like to thank Dr S. Bozhenkov and Dr A. Mlynek for many helpful discussions. This work has

been carried out within the framework of the EUROfusion Consortium and has received funding from the Euratom research and training programme 2014-2018 under grant agreement No 633053. The views and opinions expressed herein do not necessarily reflect those of the European Commission.

- ¹F. M. Levinton, R. J. Fonck, G. M. Gammel, R. Kaita, H. W. Kugel, E. T. Powell, and D. W. Roberts, *Physical Review Letters* **63**, 2060 (1989).
- ²J. Howard, *Plasma Physics and Controlled Fusion* **50**, 125003 (2008).
- ³O. P. Ford, J. Howard, and R. C. Wolf, *Review of Scientific Instruments* **86**, 093504 (2015), <http://dx.doi.org/10.1063/1.4929873>.
- ⁴O. P. Ford *et al.*, in *Proc. of the 40th EPS Conference on Plasma Physics, Espoo, Finland*, O2.110 (2013).
- ⁵A. Burckhart *et al.*
- ⁶D. Wróblewski and R. T. Snider, *Phys. Rev. Lett.* **71**, 859 (1993).
- ⁷M. Yamada *et al.*, *Review of Scientific Instruments* **63** (1992).
- ⁸H. R. Koslowski, *Fusion science and technology* **47**, 260 (2005).
- ⁹C. Petty *et al.*, *Nuclear Fusion* **42**, 1124 (2002).